applied sciences

MDPI

Article

Dynamic Stiffness Measurements of Road Pavements by Means of Impact Hammer in a Non-Resonant Configuration

Matteo Bolognese [1,*,†], Erica Greco [2,†], Francesco Bianco [3] and Gaetano Licitra [1,2,*]

[1] Pisa Department, Environmental Protection Agency of Tuscany Region (ARPAT), Via Vittorio Veneto 27, 56127 Pisa, Italy
[2] DIIES Department, University Mediterranea of Reggio Calabria, 89124 Reggio Calabria, Italy
[3] iPOOL S.r.l., Via Antonio Cocchi 7, 56121 Pisa, Italy; francesco.bianco@onda-quadra.it
* Correspondence: m.bolognese@arpat.toscana.it (M.B.); g.licitra@arpat.toscana.it (G.L.)
† These authors contributed equally to this work.

Abstract: The different sources of noise in a vehicle have long been known, and they include noise from the engine and other mechanical parts, aerodynamic noise, and rolling noise. More specifically, the latter concerns the interaction between the tire and the road surface, and so it is also known as Tire–Road Noise (TRN). One of the parameters influencing TRN is pavement stiffness. The empirical measurement of pavement stiffness, and in particular, its frequency spectrum (dynamic stiffness), is not easy to determine, and only in the last decade have studies emerged about this subject. In these works, two different instrumental chains are employed as follows: the impact hammer one and the dynamic exciter (shaker) one, which has established itself over time as a reference. The objective of this work is to develop a system for the dynamic stiffness measurements of road pavements using the impact hammer capable of producing a similar performance to the shaker while minimizing costs. During the work, a measurement aid device named Test Automation Device (TAD) was designed and implemented to increase the quality of the measurements. In line with the practical execution of the measurement, the analysis and the representation of the results were optimized to obtain results that adhere to the stiffness model proposed in the literature. In the present paper, the TAD, the measurement optimization work, the data analysis performed, and the proposed representation method will be described. Finally, we will present the results obtained and possible future perspectives.

Keywords: mechanical impedance; crumb rubber; low-cost; calibration

Academic Editors: Claudio Guarnaccia, Domenico Rossi and Edoardo Piana

Received: 7 November 2024
Revised: 23 December 2024
Accepted: 8 January 2025
Published: 10 January 2025

Citation: Bolognese, M.; Greco, E.; Bianco, F.; Licitra, G. Dynamic Stiffness Measurements of Road Pavements by Means of Impact Hammer in a Non-Resonant Configuration. *Appl. Sci.* **2025**, *15*, 651. https://doi.org/10.3390/app15020651

1. Introduction

Noise is an important environmental issue affecting a large part of the European population. Prolonged exposition to noise may affect health [1–7] or cause annoyance [8–10] and sleep disturbances [11]. Among different noise sources, road noise is one of the most impactful. In Europe, the Environmental Noise Directive (END) [12] prescribes the periodical noise mapping of main road infrastructures to monitor citizen's exposure to noise, while the member states themselves have enacted laws to set noise emission limits for infrastructures. Thus, road noise emission reduction is an important research topic.

The sound emitted from the vehicles come from the following three different sources: engine and mechanical noise; aerodynamic noise; and rolling noise, on which this work focused. Indeed, rolling noise is the most important for speeds over 40 km/h concerning lightweight vehicles and for speeds over 60 km/h concerning trucks and other heavy vehicles [13]. Rolling noise is generated by the interaction between the tire and the road

pavement, and it is affected by several noise generation, amplification, and modification mechanisms. In particular, the pavement characteristics are the most interesting because they can be defined in the design phase by technicians, while tire properties vary from vehicle to vehicle, leading to the average behavior. For this, the European Commission recently issued a regulation setting the minimum requirement in terms of noise for road paving within public procurement [14]. So an understanding of the parameters involved in rolling noise is crucial. Over the years, those relationships have been investigated; however, a complete and comprehensive understanding of all the involved parameters, especially with regard to pavement stiffness, is yet to be achieved.

Dynamic stiffness (DS) is an important parameter for road pavement resistance to stress, but it is also correlated with rolling noise [15]. The stiffness of a material is a measure of its resistance to elastic deformation and is defined as the ratio of the applied force to the resulting displacement. Considering a sample with surface Σ and thickness l, the stiffness s can be defined as follows:

$$s = \frac{F}{\Delta l} \text{ [N/m]} \quad (1)$$

where Δl is the thickness variation produced by the force F. The stiffness is also linked to the elastic modulus so that the following stands:

$$s = \frac{E\Sigma}{l} \text{ [N/m]} \quad (2)$$

where E is the elastic or Young modulus, defined as the ratio between stress σ and axial strain ε:

$$E = \frac{\sigma}{\varepsilon} = \frac{F}{\Sigma}\frac{l}{\Delta l} \text{ [N/m}^2\text{]} \quad (3)$$

Stiffness influences impact noise generation mechanisms and the transmission of vibrations between the road surface and the tire [16]. In the last two decades, several scientific and independent research projects have reported evidence that lower DS can reduce TRN [15–25].

A very similar quantity to DS is the mechanical impedance (MI), defined as the ratio between force and velocity. MI is correlated with the elasticity of the pavement and its energy dissipation capability, and it was seen that it has an effect on noise emission between 600 and 1600 Hz [26,27]. Regardless of the number of works reporting the effect of DS and MI on TRN, all those results are not yet supported by a universally accepted and validated theoretical model. To validate a DS-TRN model, a large amount of reliable pavement DS measurements is needed, but at the moment, this is limited. The reasons are mainly the absence of a standardized methodology and the technical difficulties related to the measurement itself.

The pavement stiffness measures can be classified into static or dynamic stiffness measurements. The static or quasi-static stiffness measure is well-consolidated technique [28] and is related to the stimulation of the sample at very low frequencies (less than 25 Hz [29]). In contrast, the dynamic stiffness (DS) measure is related to the frequency response of the pavement at higher frequencies (typically around the range of interest of rolling noise), and its technique is yet to be perfected, both in situ and in the laboratory.

In the last decade, several articles were published trying to adapt preexisting measurement techniques to pavements [30] or to develop novel techniques or novel indicators [18]. One of the most widely adopted methods is that indicated in ISO 9052-1:1989 [31] for measuring the stiffness of resilient materials, which are characterized by lower levels of DS compared to pavements. The measurement technique proposed by the standard is called resonant, as it is based on the mass–spring system. The test sample acts as a spring

while the role of the mass is performed by a metallic plate; thus, by knowing the resonance frequency of the system, it is possible to derive the stiffness of the sample.

Subsequently, studies have been conducted using a measurement technique called non-resonant [32], which can be seen as a sub-case of resonant measurements where the ratio between the sample's stiffness and the weight of the load plate is big. In this regime, by stimulating the sample with a force and measuring its response in terms of displacement, it is possible to derive the stiffness of the material. The stiffness's frequency response is obtained by stimulating the specimen at multiple frequencies. Using samples of elastomeric material, it has been experimentally demonstrated that this method is equivalent to the resonant one [33]. Furthermore, due to the fact that it does not require the installation of a loading mass, the non-resonant method is more practical.

Both of those techniques can be executed by two different instrumental chains for two different force signal generation. The simplest chain implies the usage of an impact hammer that allows for generating impulsive force signals (ISO 7626-5:2019 [34]). The most complex one, already established as the standard measurement chain in the field of modal analysis, implies the usage of a dynamic exciter or mechanical shaker, also known as "shaker", that can generate sinusoidal and pseudo-chaotic force signals ISO 7626-2:2015 [35].

Earlier work applying these techniques to road pavements used an impulsive force. Following results that are not too encouraging, some authors introduced the use of the shaker, which by generating sinusoidal signals allows for a higher signal-to-noise ratio. Then, after a number of studies utilizing the shaker were carried out, some authors [36] have successfully applied the non-resonant technique to road pavements and have proposed a model for the frequency response of DS. They, however, argue that the same results cannot be obtained using the instrumented hammer.

The shaker's ability to perform the sinusoidal excitation of the sample allows is to reach high level of signal-to-noise ratio, very good stability, and good repeatability of the measurement. However, it presents some critical issues that make its usage not very practical for on-field measurements. First of all, it is expensive, difficult to transport, heavy, and requires a powerful and heavy amplifier. Secondly, to cover the desired spectrum of the DS, multiple measurements are needed or a sweep signal must be utilized, requiring a long time to execute the measurement. The alignment of the shaker is also time consuming.

On the other hand, the impact hammer generates impulses that, in theory, are capable of investigating a wide range of frequencies in one shot, and so, with far less time compared to the shaker. The hammer is also easier to transport, less expensive, and easier to use. Moreover, shaker and hammer measurements were proven to be equivalent for the measurement of DS for other types of materials [37,38], so the same should be possible for pavements. Thus, considering these arguments, effectively using the hammer in DS measurements, and being able to obtain comparable results with those of the shaker in terms of accuracy, is very attractive . Hopefully, a validated and accurate hammer methodology to measure pavement DS will finally allow us to produce the amount of DS measurements needed to understand the relationship between DS and TRN.

The present work aims to fine-tune the non-resonant method with the impact hammer to achieve similar reproducibility and accuracy to that obtained with the shaker [36] and to provide a more easy-to-use and easy-to-setup method for determining the DS of pavements. To this end, the authors designed and 3D printed a low-cost device named Test Automation Device (TAD) to perform a semi-automatic measurement and to allow for better control of the impact. Using the TAD, the limits of the handheld usage of the hammer were identified and a best practice procedure for the non-resonant road pavement DS measurement was defined. The fine-tuned measurement chain was then used to correctly reproduce the

predicted frequency response proposed in [36] , with R^2 values very close to the unity for boot in situ pavements and pavement samples.

The in situ pavements tested and the sample used for the optimization process were developed under the LIFE E-VIA (Electric Vehicle noIse control by Assessment and optimization of tire/road interaction) project. The project aims to address road traffic noise pollution by focusing on a future perspective where electric and hybrid vehicles are a substantial part of the flow.

The other sample was provided by the LIFE NEREiDE project (Noise Efficiently Reduced by Recycled Pavement), which aims to define the guidelines and best practices for the design, building, and monitoring of pavements with high environmental sustainability.

In the Sections 2 and 3 a description of the measurement principle and a brief literature review are provided. In Section 4, the methodology and the designed mechanical device are described in depth. Sections 5 and 6 describe the experimental setup and calibration. The results are then presented in Section 7, including the in situ and in laboratory measurements. A discussion of the results is then provided in Section 8.

2. Measurement of Dynamic Stiffness

As mentioned in Section 1, DS measurement techniques can be divided into two types, resonant and non-resonant. The latter is the one used in the present work and can be viewed as a subcase of the resonant method.

The first approximation of the system of the resonant method is governed by Newton's second law as follows:

$$F(t) = m\ddot{x}(t) + c\dot{x}(t) + sx(t) \tag{4}$$

where:

- c is the damping rate of the spring, equivalent to the sample damping;
- s is the spring constant, and is equivalent to the sample stiffness;
- m is the mass, and corresponds to the mass of the loading plate;

In the hypothesis of harmonic forces ($F(t) = F_0\ e^{i\omega_0 t}$), the displacement x will be $x(t) = x_0\ e^{i\omega_0 t}$, and switching to the frequency domain, we can obtain the frequency response function of the system (*FRF*) $H(\omega)$, which in this case corresponds to the compliance and is the reciprocal of the stiffness as follows:

$$H(\omega) = \frac{x(\omega)}{F(\omega)} = \frac{1}{(s - m\omega^2) + ic\omega} \tag{5}$$

The test consists of the identification of the resonant angular frequency ω_r of the system which depends on the sample stiffness and for which the compliance is at a maximum as follows:

$$\omega_r = \sqrt{s/m} \tag{6}$$

so that the stiffness k can be obtained by reversing the formula. However, the sample stiffness generally depends on frequency; thus, the obtained value of stiffness is valid only in the proximity of ω_r. Therefore, it is more correct to express stiffness as $s(\omega_r)$, making explicit the frequency dependency. This implies that, to correctly evaluate the stiffness of the sample in the entire frequency range of interest, multiple measurements must be performed by varying the load plate's mass m.

The non-resonant method can be seen as the resonant method in the limit of resonant frequency much higher than the frequency range of interest (5), $\omega \to 0$ (or $\omega \ll \omega_r$) ($m \ll \omega^2/s$).

In those conditions, the modulus of the DS can be expressed in terms of force and acceleration as follows:

$$|s(\omega)| = \frac{|F(\omega)|}{|\ddot{x}(\omega)|}\omega^2 \quad (7)$$

In contrast with the resonant method, there is no technical standard for non-resonant measurements to refer to, but the absence of the loading plate makes the method more practical and allows for it to also be applied to in situ pavements.

3. Literature Review

In Table 1, a synthetic summary of the techniques and the instruments utilized by various authors from the literature is reported. As it can be seen, there is not a pronounced preference to one technique or instrument, but the most recent articles seem to prefer the utilization of a mechanical shaker instead of hammer. Furthermore, the non-resonant technique is the most used.

Table 1. Literature articles on pavement stiffness or MI evaluation with an indication of the techniques and instruments used.

Article	Resonant	Non-Res.	Hammer	Shaker	D. Stiffness	M. Impedance
Vázquez 2012 [39]	Yes	No	Yes	No	No	No
Bendtsen 2014 [40]	No	Yes	Yes	No	Yes	Yes
Zakaria 2014 [41]	No	No	No	No	Yes	No
Vázquez 2016 [32]	Yes	Yes	No	Yes	Yes	No
Li et al. 2016 [18]	No	Yes	Yes	No	No	Yes
Vázquez 2019 [42]	No	Yes	No	Yes	Yes	No
Vázquez 2020 [36]	No	Yes	No	Yes	Yes	No
Czech 2020 [43]	No	Yes	No	Yes	Yes	No
Praticò 2023 [44]	No	Yes	Yes	No	No	Yes

The first article to the authors' knowledge that reports measurements of the DS of road pavements is [39]. In this work, the dynamic stiffness of four specimens of SMA pavements was tested by adapting the ISO 9052-1:1989 [31] to perform comparisons between results from static measurements based on EN 12697-26:2018 [28] and between results from the CPX measurements performed on the corresponding in situ paving of the same pavements. The tested pavements are differentiated by their maximum grain sizes (11 mm or 16 mm) and by the presence of crumb rubber. The frequency range of analysis for DS measurement is below 500 Hz. For three of four specimens, the results appear to indicate a correlation between the static and the dynamic results, but for the forth one (11 mm with no crumb rubber), the DS is below expectation. The CPX results were tested on a test track to evaluate noise emission from SMA 16 mm and SMA 11 mm, but the authors do not indicate if crumb rubber is present or not in the mixture. The results seem to confirm a lower emission from the 11 mm samples that resulted in lower DS, but the anomalous result of the 11 mm with no crumb rubber raises doubts about the results.

In a following work [32], the authors performs DS measurements in resonant and non-resonant configurations by mean of a mechanical shaker. The specimens tested are described in Table 2, where the corresponding values of the DS, derived by the authors by multiplying the resonant results presented in [32] using the sample area, are also presented. The value was calculated to allow for a direct comparison between the results of the two configurations. In comparing the values, we must keep in mind that the author's analysis of the spectrum was limited to 500 Hz because at this frequency, there was a resonance that seemed to invalidate the measurement for higher frequencies. As we can observe, there

is no agreement between the results for the softer materials (PU and EPS) as the values obtained with the two techniques are of different orders of magnitude.

This result would be in disagreement with what was obtained by [33], which found substantial equivalence between the two methods. A better agreement seems to be obtained for the remaining samples; however, the authors do not provide estimates of the uncertainty, so it is not possible to make a judgment on the merits of this method.

Table 2. Specimen specifications and DS results from [32].

Sample	Thickness [mm]	Resonant Frequency [Hz]	Apparent DS [MN/m^3]	DS [MN/m]	Non-Resonant DS [MN/m]
PU	2307	4.9	10.9	0.0856	0.0017
EPS	2342	4.5	81.7	0.642	0.015
SMA-C	2475	4.4	1436	11.2	12.87
SMA-H	2496	4.6	3484	27.4	17.23
Concrete	2496	4.6	4330	34.0	33.8

[1] The results in the column "DS" was calculated by the authors of the present work from the data provided in [32].

A subsequent paper [36] has refined the application of the non-resonant method to road pavements and has applied it to in situ pavements. The data provided by the authors on the tested pavements are shown in Table 3. The authors extend the analysis up to 4 kHz, obtaining the same resonance evidenced in their previous works [32,42] and by other authors [18]. To bypass the resonance problem, the authors propose the following model for the DS:

$$s(f) = A_2 + \frac{A_1 - A_2}{1 + \exp\left(\frac{f - f_0}{df}\right)} \quad (8)$$

where

- A_1 is the minimum stiffness;
- A_2 is the maximum stiffness;
- f_0 is the median frequency between A1 and A2;
- df is the envelope frequency width.

As it can be seen from [36], the results exhibit substantial agreement with the model.

Table 3. Pavement specifications from [36].

Pavement	Aggregate Size [mm]	Bitumen Content [%]	Void Content [%]	Density [kg/m^3]	Age
BBTM11	11	5.2	6.7	2430	2 months
BBTM11 CR	11	8.3	5.7	2326	2 months
CIR	22	5.3	12.0	1851	2 months
SMA8	8	5.7	4.9	2382	2 months
AC16	16	5.0	4.2	2355	10 year

In [44], the first application of the mechanically controlled hammer to road pavements is presented together with a preliminary study. The authors, after testing the effect of different configurations of hammer tips, bitumen mixtures (with and without crumb rubber content), and force application in the MI spectrum, were not able to reproduce similar results to those obtained with the shaker in [36].

4. Methods and the Representation of Results

To provide better control over the hammer impact and to prevent the hopping effect, a test automation device (TAD) was designed and 3D printed. The designed device is depicted in Figure 1, in the configuration for in situ measurements. The device consists of a main structure, a sleeve for attaching the hammer, a support structure, a counter-reaction spring, and a force regulator.

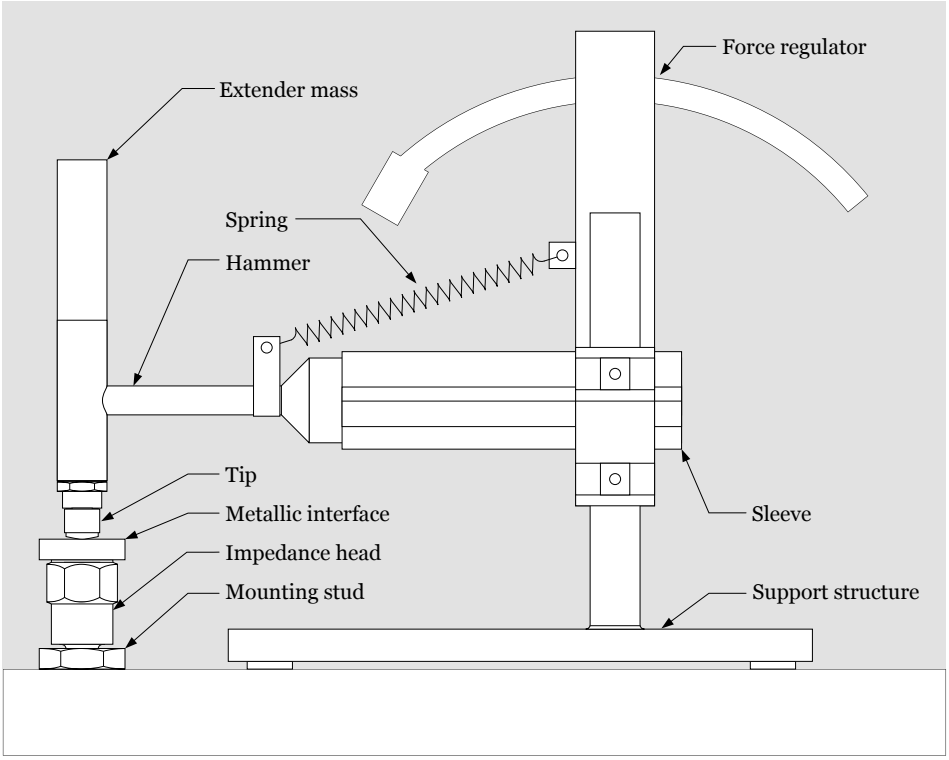

Figure 1. Example of the experimental setup in the case of in situ measurement. The impedance head is attached to the ground via a threaded mounting stud in this case. The impact hammer, the impedance head, and TAD are depicted. For illustrative purposes, the optional weight was included for the hammer.

The hammer is attached to the structure by a sleeve, which is pivoted to the main structure so that it can rotate around a single axis. The main structure integrates a mechanism for impact force regulation, which essentially consists of an arc with an adjustable circumference that has the function of a hard stop, that is, a limit for the rotation of the hammer and sleeve. Its effect is to limit the maximum height at which the operator can lift the hammer and, thus, the resulting impact force. Indeed, the measurement is made by manually lifting the hammer to the angle allowed by the limit and letting it fall back on the impedance head. The counter-reaction spring is properly attached to the hammer and to the structure to provide the appropriate counter-reaction and prevent hopping after the initial impact.

As can be seen in Figure 2, there are actually two impact angles, the angle between the axis of the hammer handle and the ground plane and the angle between the axis of the hammer head and the vertical axis. The control of those angles is achieved by adjusting the height of the main structure along the bracket and adjusting the rotation of the hammer in the sleeve seat.

A typical DS spectrum obtained with the hammer in combination with the TAD is reported in faded gray in Figure 3. The figure presents the three spectra corresponding to three independent in situ measurement sessions on the same road surface point. In light

blue, the medium 1/3 octave band spectrum of the three results is reported, while in orange, the sigmoidal model proposed by [36] is shown. Below the 1 kHz band, there is a complete overlapping between the 1/3 spectrum, the model, and the three fine band spectra . For higher frequencies, the three fine band spectra are subjected to variation from the model, but they overlap themselves. Starting from 2500 Hz and above, the three spectra begin to be subjected to random oscillations which are not overlapping. Otherwise, the medium 1/3 octave band spectrum mitigates this behavior, exhibiting very good agreement with the model. Based on that evidence, the authors propose representing the DS spectrum results in 1/3 octave bands to enhance the readability of the results and to facilitate fitting with the sigmoidal model from the literature (Equation (8)). The DS third-octave spectrum is obtained by averaging the spectra of three independent measurements performed on the same measurement point. The spectrum of each measurement is calculated from the narrow-band spectrum obtained from ten consecutive impacts following the ISO 7626-5:2015 [34]. The error bars associated with the band's value of the medium spectrum represent the standard deviation between the three original spectra.

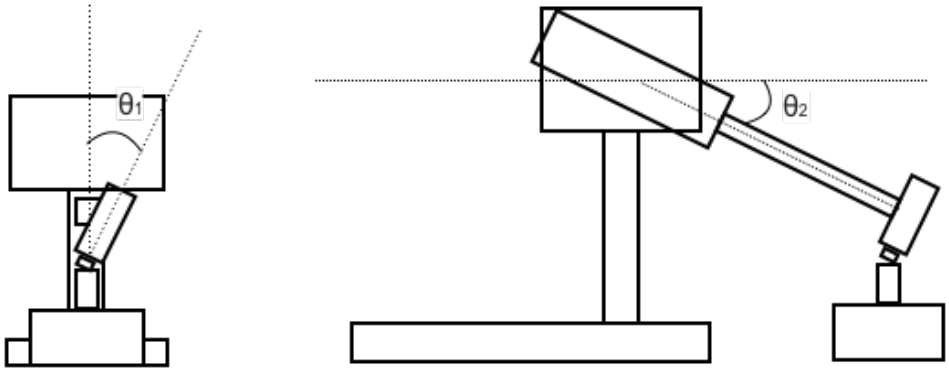

Figure 2. Depiction of the angles of impact. The angle θ_1 is the angle between the hammer head axes and is perpendicular to the ground, while θ_2 is the angle between the hammer axes and the ground plane.

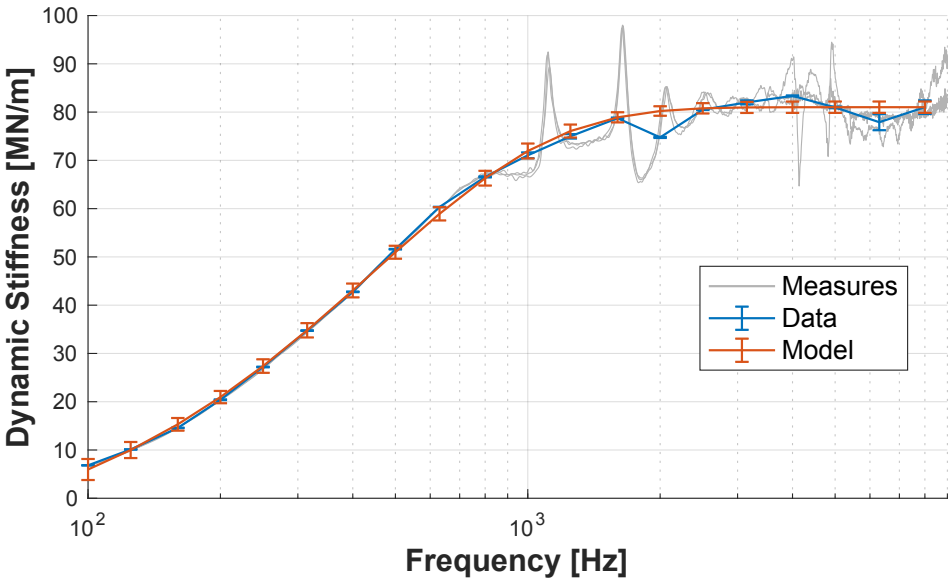

Figure 3. Fit of the trend in 1/3 octave bands with the sigmoid model. Shaded in gray are the frequency spectra of the stiffnesses measured in the three individual measurements. At a low frequency, the unmediated trend is in agreement with the model. At a high frequency, the trends of the three measurements are no longer superimposable, but averaging over the band still allows for good agreement with the model.

5. Experimental Setup

The instrumental setup used in the present study is the following:

- Impact hammer AU02;
- The Test Automation Device TAD;
- Impedance head DJB AF/100/10;
- A NI acquisition board (NI9234-based);
- A laptop with Labview acquisition software.

In Figure 4, the setup is depicted in the configuration of in-laboratory measurements. In Figure 1, the details of the TAD are reported in the configuration of the in situ measurements (the impedance head is directly attached to the pavement surface in this case). The technical specifications of the hammer and impedance head are reported in Tables 4 and 5, respectively. The impulse characteristics based on the hammer configurations are reported in Table 6.

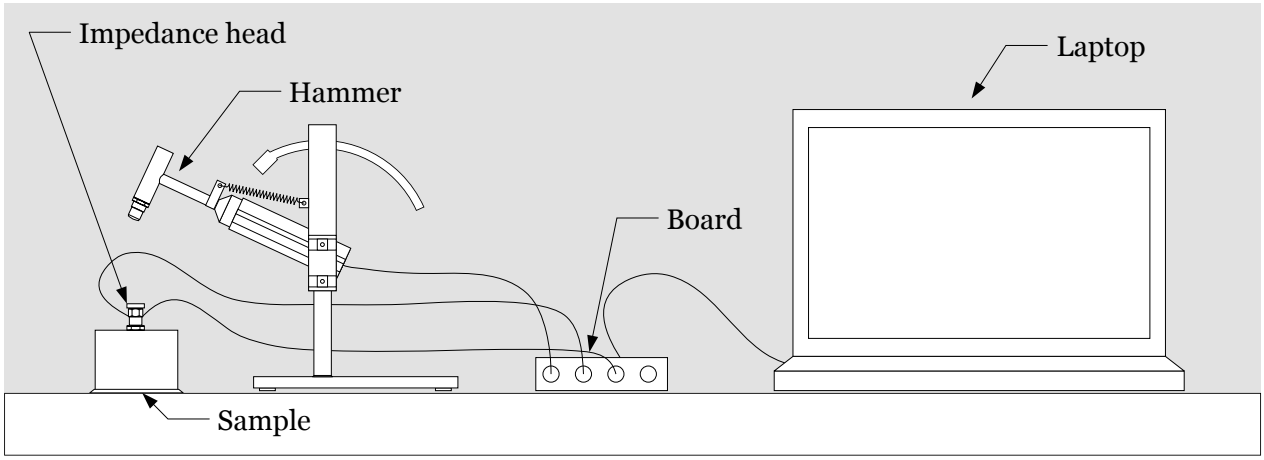

Figure 4. The experimental setup in the case of the dynamic stiffness measurement of pavement specimens in the laboratory.

Table 4. Spreadsheet of the impulse hammer AU02 from the ROGA instruments.

	AU02
Transducer	AC21
Sensitivity [mV/N]	1.5
Transverse sensitivity	<5%
Force range [N]	$-1000 + 5000$
Resolution [N]	0.003
Hammer mass [g]	330
Mass of steel tip [g]	10
Mass of rubber tip [g]	9
Mass of nylon tip [g]	7
Mass of extender [g]	108

Table 5. Technical specification of the impedance head DJB AF/100/10.

	AF/100/10
Manifacturer	DJB
Sensitivity force ($\pm$10% @ 20 C) [mV/N]	10
Sensitivity acc. ($\pm$10% @ 20 C) [mV/g]	100
Measuring range force [N]	500
Measuring range acc [m/s^2]	$\pm$490

Table 5. *Cont.*

	AF/100/10
Typical frequency range force [Hz]	0.7–6 k
Typical frequency range acc. (±5%) [Hz]	1–6 k
(±10%) [Hz]	0.7–8 k
Weight [g]	30

Table 6. Characteristics of the impulse produced by the hammer in different configurations of tips and extenders.

Configuration	Force Range [N]	Shock Duration [ms]
Steel tip	500–5000	0.1–0.2
Steel tip and extender	500–5000	0.15–0.3
Rubber tip	300–1000	0.4–0.6
Rubber tip and extender	300–1000	0.5–0.8
Nylon tip	100–700	1.2–2.6
Nylon tip and extender	100–700	1.7–3.9

6. Calibration

The ISO 7626-5:2019 [34] used for the impact hammer measurements requires system calibration before and after each measurement. According to the standard, the procedure consists of measuring the acceleration, or rather the mobility of a rigid block of known mass under "*freely suspended*" conditions. The "*freely suspended*" condition is satisfied when the sample is suspended via a support structure and the mobility of the sample-side anchor point is at least 10 times greater than the mobility of the structure-side anchor point.

There are at least two different strategies used to satisfy this condition, both of which were tested during the present work. The first involves the elastic suspension of the calibration mass; the second involves a pendulum with an appropriate period of oscillation. In each case, based on [34], the conditions to be met are as follows:

- The frequency response of the calibration block must be compatible with its expected value with a 5% tolerance in the frequency range of interest as follows:
  - In our case, the magnitude of the acceleration must be 1/m where m is the mass of the calibration block;
- The mass of the block should be chosen to reproduce the range of acceleration measured during the tests;
- The calibration procedure should be repeated at the beginning and at the end of each measurement session and for each change of hammer tip or mass.

Compliance with the 5 % tolerance must be achieved by assigning a known calibration coefficient to the accelerometer signal and properly adjusting the calibration coefficient for the impact hammer. If the acceleration value measured during calibration is not approximately constant over the frequency range of interest, the procedure prescribes considering the test null and investigating the possible causes of such behavior. Regardless of the ISO requirements, there is no reference to calibration in the published literature to the authors' knowledge.

In the following paragraphs, we will describe both the calibrations performed and the results obtained, as well as the results of the acceleration signal calibration.

6.1. Calibration of the Acceleration Transducer

Before calibrating the hammer, or the force sensor in general, it is necessary to perform a calibration of the acceleration sensor, which in our case is the accelerometer inside the

impedance head. This calibration was performed by means of a reference shaker calibrator (Kistler, type 8921B02, Winterthur, Switzerland) with fixed frequencies between 80 Hz and 1280 Hz. The calibrator is capable of generating a sinusoidal acceleration with a known RMS value, in our case equal to 10 m/s^2. The acceleration measured by the impedance head was then recorded to calculate the measured RMS value. Table 7 shows the measured RMS values for each frequency and the corresponding calibration factor. In Figure 5, the results compared with the tolerance intervals are also reported. The acceleration signal is correctly calibrated in the frequency range that can be investigated with the calibrator. Unluckily, the available calibrator was not capable to investigate the whole frequency range of interest, so this aspect can be improved in future works.

Table 7. Impedance head calibration results. Calibration values are calculated with respect to the RMS reference acceleration value of 10.00 m/s^2.

Frequency [Hz]	RMS [m/s^2]	Calibration Value
80	10.36	0.965
159	10.30	0.970
320	10.26	0.974
640	10.16	0.983
1280	10.38	0.962

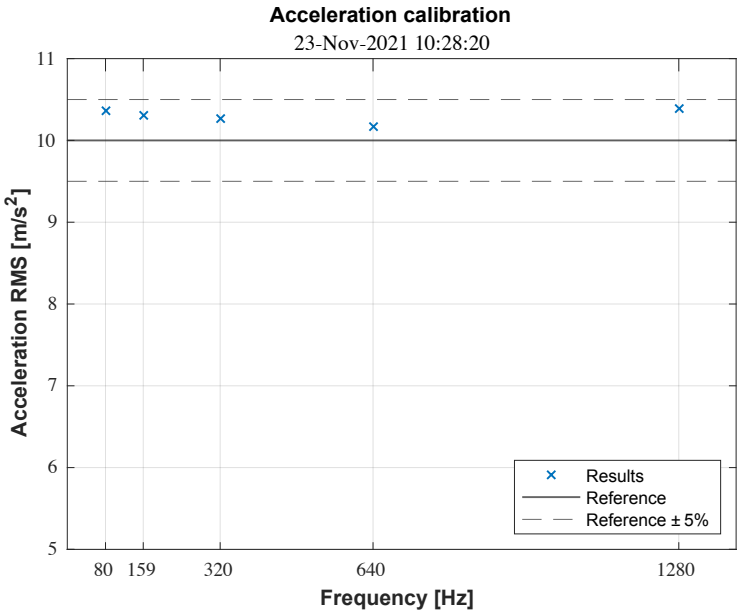

Figure 5. Calibrazion results for the impedance head.

6.2. Calibration of Force Transducer

During our work, the calibration of the hammer was performed with two different configurations reproducing *freely suspended* conditions. The first one, depicted in Figure 6, uses the elastic suspended mass and allows the hammer to be calibrated using the TAD. The obtained results are presented in Figure 7.

The second one is based on a pendulum and is not recommended for the calibration of the hammer in combination with the TAD because it requires the manual use of the hammer. The obtained results are presented in Figure 8. As can be seen from the figures, the two methods tested perform differently. The elastically suspended calibration could provide acceptable calibration results in the range 100–1k Hz, but the spectrum is not flat.

The pendulum-like calibration instead produces a more uniform dynamic mass response, but the calibration is possible only below 400 Hz.

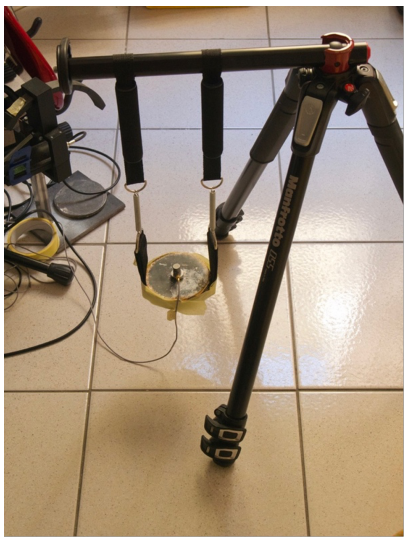

Figure 6. Calibration structure for setup calibration using elastic supports.

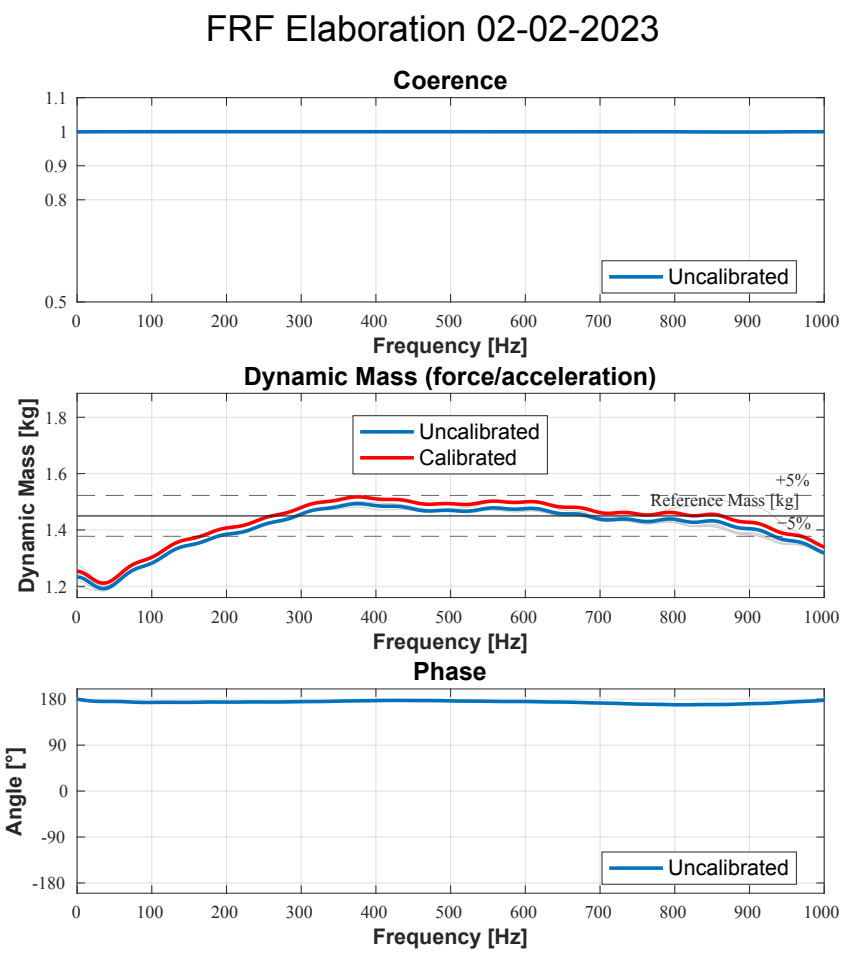

Figure 7. Calibration results with the elastic calibration setup. The original curves are shown in gray, the average trend used for calibration is shown in in blue, and the calibrated average using as coefficient the average value of $m(f)$ between 100 Hz and 1000 Hz is shown in red.

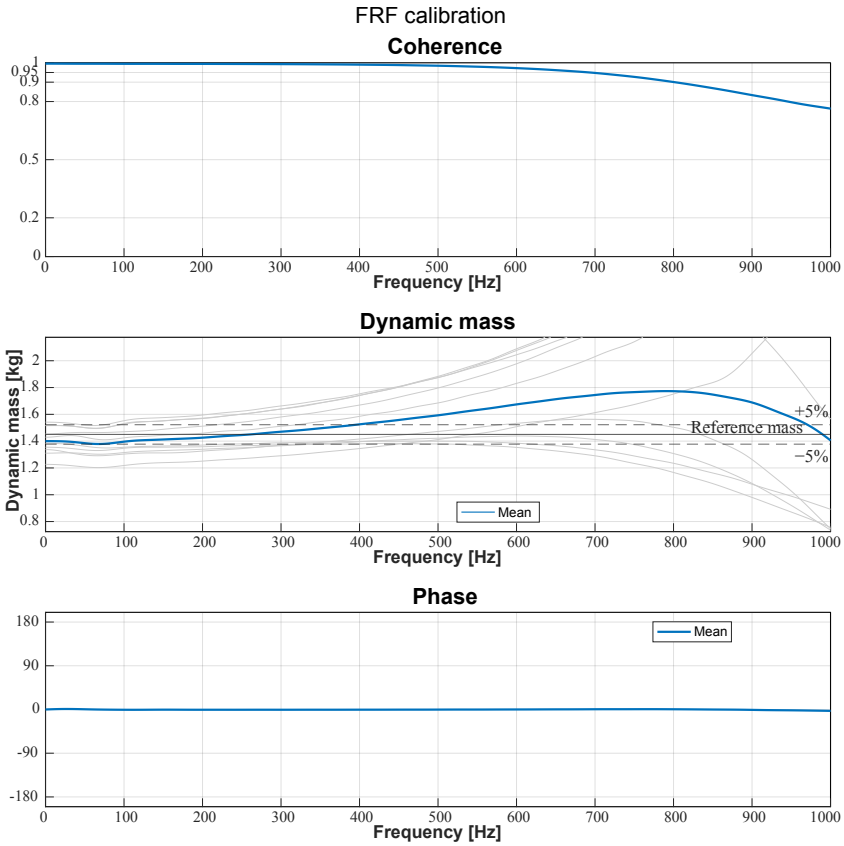

Figure 8. Calibration results with the pendulum calibration setup.

7. Results

In this section, the results will be presented, starting from the tests performed to find the criticality of the manual execution of the non-resonant method on pavements and to define a refined methodology. Those tests were conducted on a pavement specimen from the LIFE E-VIA project.

Later, two DS measurements on crumb rubber pavements will be presented. The first is a in situ measurement performed on the experimental road surfaces on the "via Paisiello" experimental site in Florence, taken from the E-VIA LIFE project. The second one is an *in-lab* measurement of a sample from the LIFE NEREiDE project.

7.1. Optimization Process with In-Laboratory Measurements

The study of the influence of installation conditions and the impact parameters on the measurements was carried out on a pavement sample with crumb rubber-modified bitumen, taken from the E-VIA LIFE project. The specimen characteristics are provided in Table 8. In the present subsection, the obtained results will be presented.

Table 8. Technical specifications of pavement sample, *c8-2%*, used for tuning the measurement system.

	AC6d 8 2% RARX T
Rubber content [%]	1.88
Bitumen content [%]	6.20
Weigh [g]	657.53 ± 0.01
Diameter [mm]	97.5 ± 0.5
Heigh [mm]	38 ± 1
Bulk specific gravity	2.338
Maximum gravity	2.377
Porosity [%]	1.63
Marshall stability [Kg]	1536.04
Marshall quotient [kg/mm]	296.13

7.1.1. TAD vs. Manual Hammer

A comparison between the manual usage of the hammer and the use via the TAD was conducted and reported in Figure 9 with results up to 8 kHz. Third-octave bands with a deviation higher than 10% or with a coherence between 0.2 and 0.9 are depicted with a lighter color to better highlight criticality.

The manual usage results in very high variations under all the 1/3 octave bands while the TAD results are characterized by a low level of variation (under 10%), except for the 1600 Hz band. The band value trend is also less affected by variation under the 4 kHz band. To estimate the force variation under the two uses of the hammer, a statistical study was conducted after performing 100 strikes, subdivided into 10 independent sessions, using the two techniques with a force target of 100 N. The force distributions over the 100 strikes are reported in Figure 10, where the great dispersion of the manual results compared with the results obtained with the TAD can be seen.

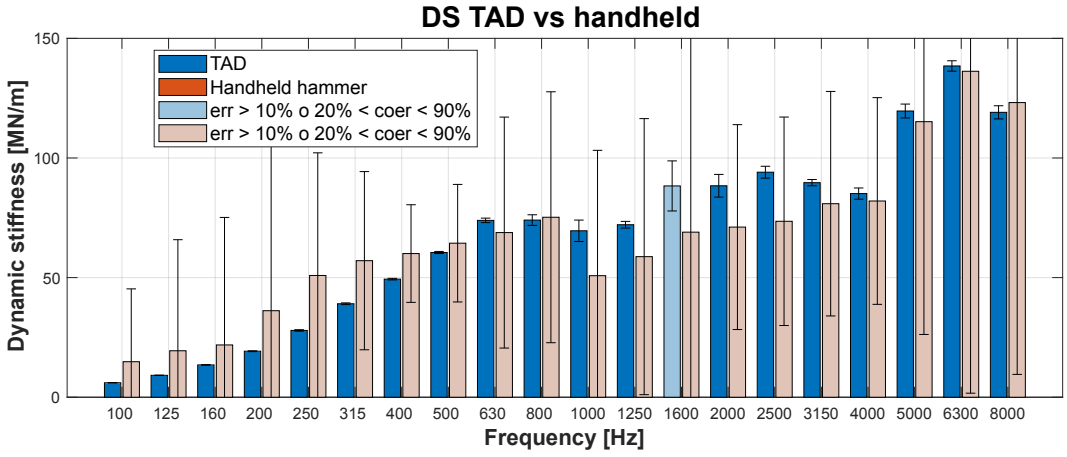

Figure 9. Comparison of the dynamic stiffness trend in third-octave bands between the mechanical method, in blue, and the manual method, in red.

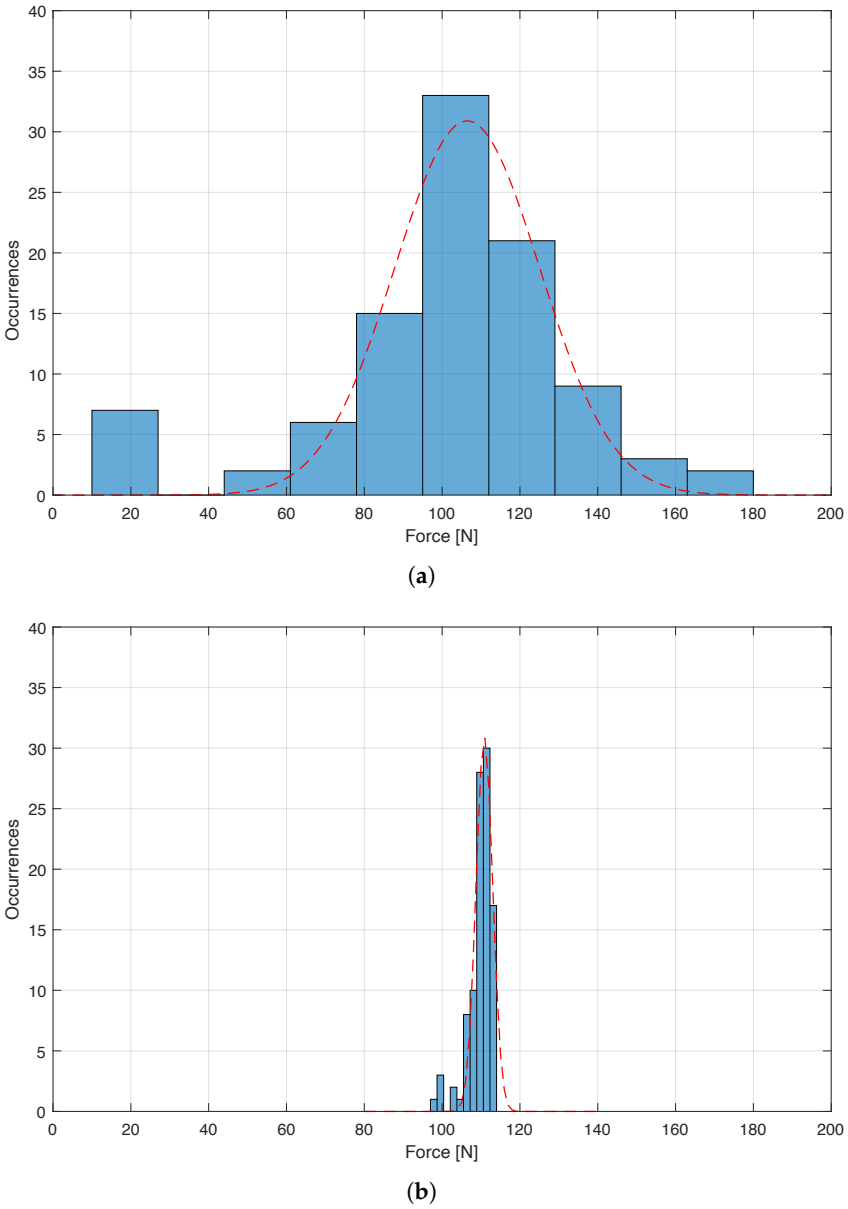

(**a**)

(**b**)

Figure 10. Force distributions by the manual (**a**) and the mechanized (**b**) method using the TAD.

7.1.2. Linearity Test

To test the dependence of the measured DS on the applied force, two measurement sessions were conducted varying the applied force in the range of 20–220 N, separately fastening the sample with plaster and concrete. The results presented in Figure 11 show that for a force lower than 100 N, the plaster offers a lower variability of results, but in the rest of the range, the concrete results are more constant with the variation of the force.

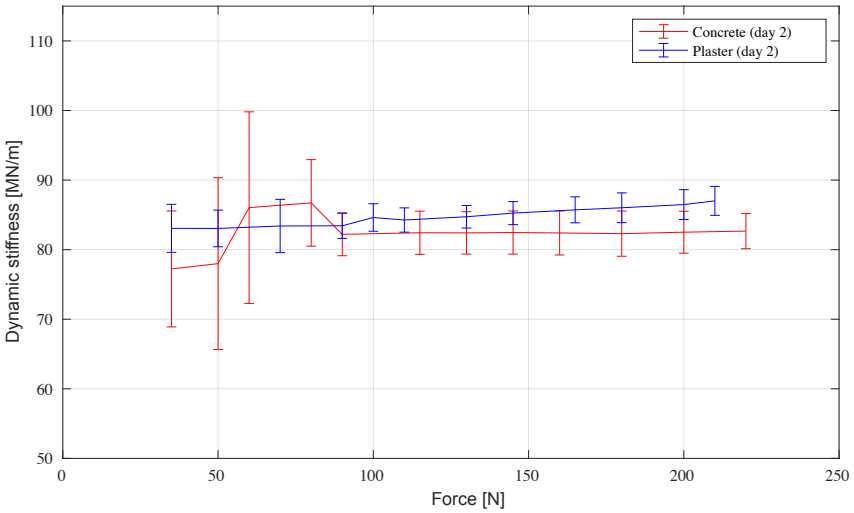

Figure 11. Trend of dynamic stiffness as a function of the applied force. In red, the trend on the specimen fixed with concrete is shown, and in blue, the trend on the specimen fixed with plaster is indicated.

7.1.3. Impact Angle Influence

Two separate studies were conducted to evidence the influence of the two impact angles from Figure 2 to the DS results. In Figure 12, the results in terms of fit parameters are reported.

In the two cases, increasing the impact angles leads to a R^2 reduction, while the confidence interval (δs) generally increases. The DS estimation value instead remains almost constant under 15°, but it is subjected to more important oscillation in larger angles.

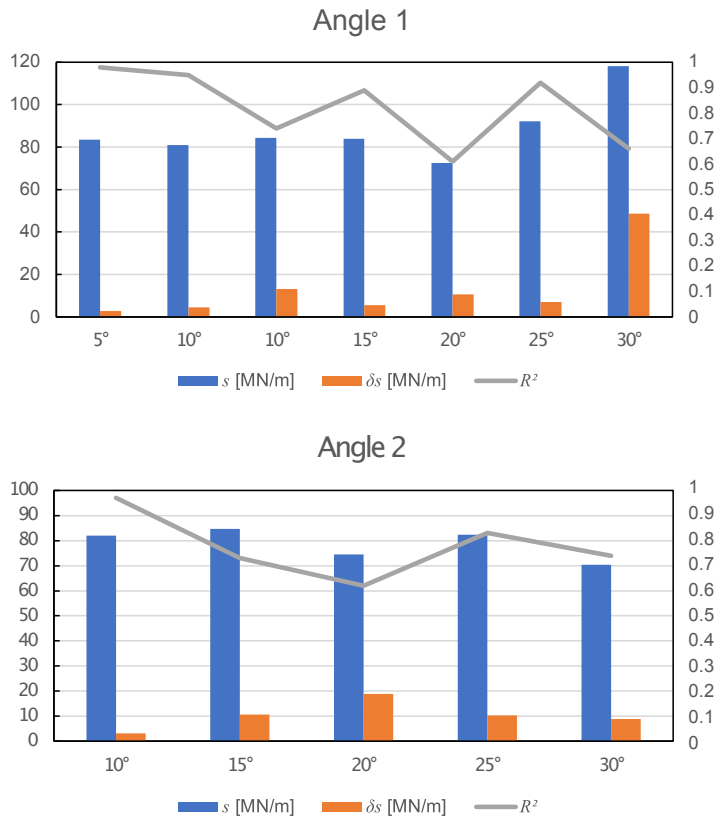

Figure 12. Influence on DS (s), associated confidence interval (δs), and the R^2 coefficient based on the two angles of impact.

7.1.4. Sample Placement

Three measurement sessions were conducted on sample fastening using concrete, and two sessions were conducted to monitor plaster drying. The concrete fastening measurement sessions were as follows:

- Session 1: 19 May–30 May 2022, the stiffness measurement was performed on days 1, 5, 6, 7, 9, and 12 from the day of fastening;
- Session 2: 31 May–9 June 2022, the stiffness measurement was performed in 1, 2, 4, 5, and 6 hours from fastening and then on the following days: 1, 3, 6, 7, 8, 9, 10;
- Session 3: 28 June–4 July 2022 stiffness measurement was performed on days 1, 2, 3, 4, and 7 from the day of sample fastening.

Plaster fastening measurement sessions:

- Session 1: 14–16 June 2022. The sample was set on 13 June and monitored on the following drying days: 1, 2, 3. At the end of the measurement on the third day, the sample lost adhesion and was found to be disconnected from the gypsum layer, so monitoring was stopped.
- Session 2: 12–14 July 2022. The sample was set on 11 July and monitored on the following drying days: 1 and 3. Thereafter, the sample lost adherence.

Figure 13 shows the results of the drying processes. Regarding concrete fastening, as expected, in the first hours after laying (Cement Session 2, in red), the stiffness values are lower because the cement is not yet very solid. Hardening is achieved as early as the first day of drying, and valid measurements should be those taken from day 1 through day 7. For concrete Sessions 1 and 2 (red, blue) from day 7 onward, there is a gradual decrease in stiffness, hypothetically due to the fact that the specimen is beginning to detach from the cement layer. For Session 3, the decrease takes place as early as day 4. In the case of plaster fastening, however, monitoring was performed from the first to the third day of drying in two measurement sessions (in green and black). The plaster's monitoring sessions show stiffness values comparable to each other and to those obtained in the cement drying sessions. In addition, those results appear to provide greater measurement repeatability than those obtained using concrete.

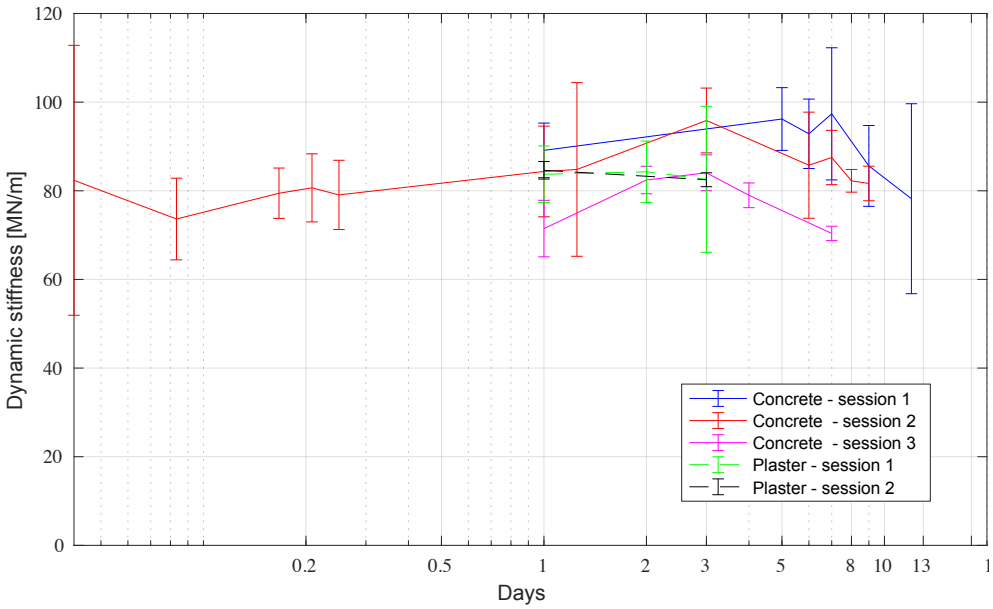

Figure 13. Trends in dynamic stiffness as a function of drying days for all five sessions. The x-axis is on a logarithmic scale because in Concrete Session 2 (in red), monitoring was also performed for the first few hours after fixation, unlike the others where daily monitoring was performed.

7.1.5. Hammer Configuration

A comparison was conducted between the usage of two different hammer tips, the rubber one and the nylon one. The results reported in Figure 14a show a negligible difference between the two tips, with exception of the 1600 Hz band, where the nylon tip exhibits a standard deviation greater than 10%.

Furthermore, the effect due to the utilization of the extender mass was investigated and reported in Figure 14b.

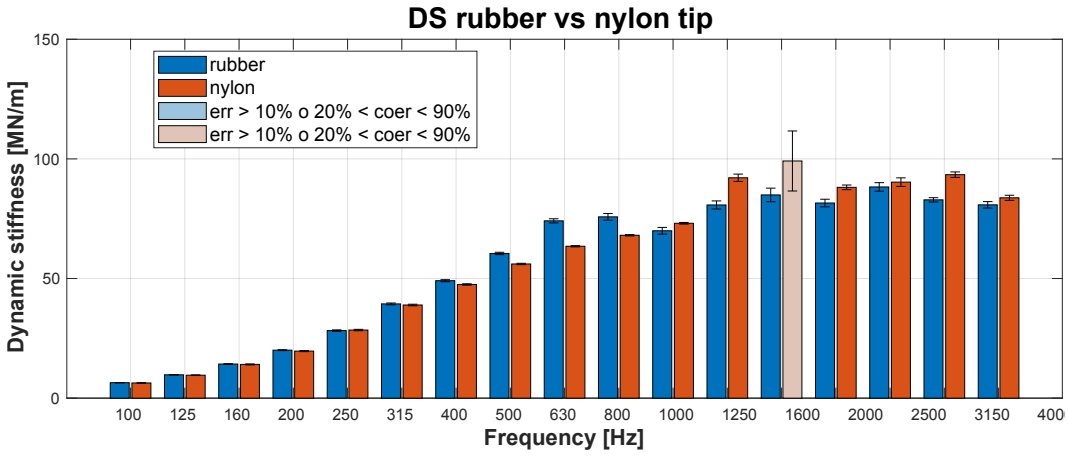

(**a**)

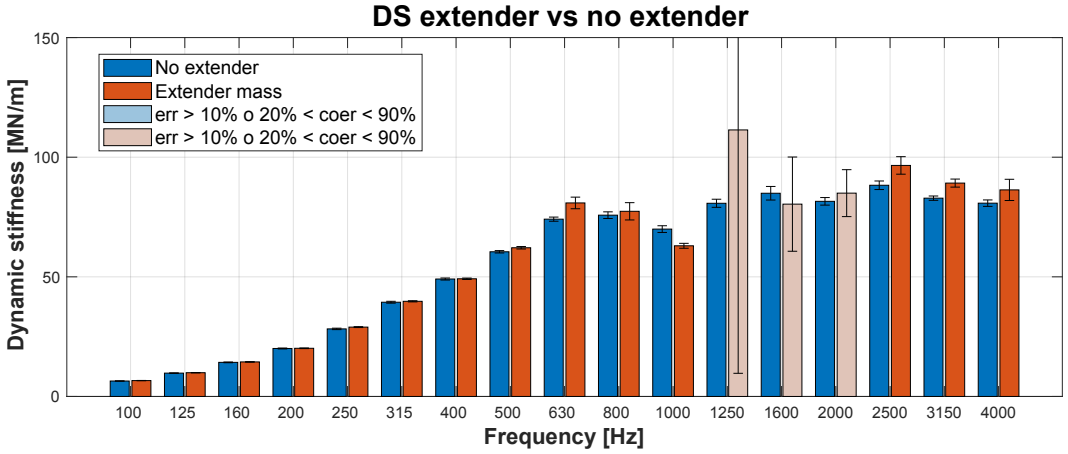

(**b**)

Figure 14. Effect on DS measurements of the tip and mass extender. (**a**) Tip effect on the DS results. (**b**) Extender influence on DS results.

7.1.6. Impedance Head

A study to investigate the advantages provided by the interposition of a metallic interface on top of the impedance head was conducted and reported in Figure 15a.

Without the interface (in red), the measurement is less stable and accurate because of the hole in the impedance head. Indeed, there are three bands in which the standard deviation is greater than 10%. In particular, the 1 kHz band shows very high variability, which can be attributed to the presence of resonance. As expected, the metal interface makes the DS spectrum 'cleaner' and the measurement more accurate, avoiding the problem of disturbance due to the presence of the hole.

The influence of the impedance head fastening methods to the sample/pavement was also investigated, comparing screwed fastening and magnetic fastening. The results are reported in Figure 15b.

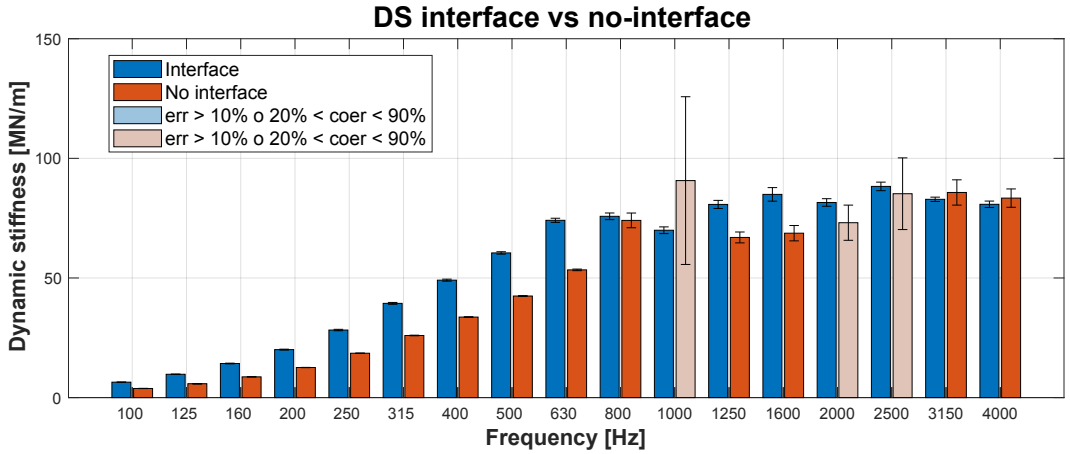

(**a**)

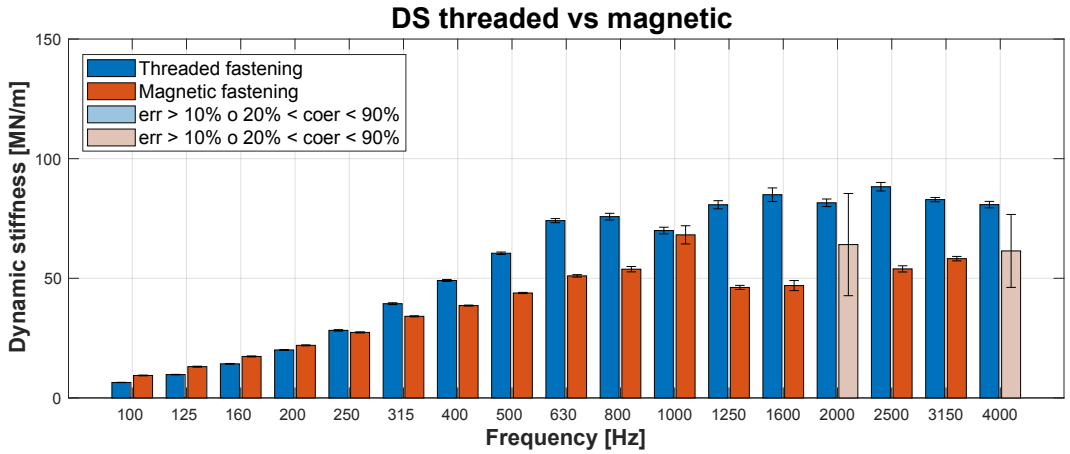

(**b**)

Figure 15. Effect of the fastening methods and the presence of superficial irregularities on the impedance head. (**a**) The third-octave band DS spectrum without the metal interface (in red) and with the metal interface (in blue) to avoid disturbance due to the presence of the hole on top of the impedance head. (**b**) Comparison of different fastening methods used for the impedance head.

Based on the results presented, it is possible to draw up the following list of practical indications for carrying out the measure:

- Concrete or plaster fastening should be preferred based on the external condition (for in-laboratory measurements);
- Measurement should be performed between 24 and 48 h from the sample laying (for in-laboratory measurements);
- The screwed fastening of the impedance head must be utilized;
- An appropriate metallic interface must be installed on top of the impedance head;
- A rubber tip should be preferred;
- A target for the impressed force should be set to 100 N;
- The use of a mass extender is not recommended;
- The impact hammer must be properly aligned, thus, leveling the system before each measurement is mandatory.

These guidelines were followed to obtain the results presented in the following subsections.

7.2. Results for In-Laboratory Measurements

In this section, the DS result obtained on a sample of crumb rubber modified bitumen sample from the LIFE NEREiDE project is presented. The sample is characterized by a

high level of crumb rubber content and it was built using the *"wet"* method. The technical specification of the sample and the measured DS results as well as the resulting Young modulus are reported in Table 9. The DS spectrum is also reported in Figure 16.

Table 9. Technical specifications and DS results of pavement sample *M2I* from the LIFE NEREiDE project.

	M2I Gap Dry
Rubber content [%]	3.0
Bitumen content [%]	8.0
Porosity [%]	10.5
Weigh [g]	924.3 ± 0.1
Diameter [mm]	100.0 ± 0.5
Heigh [mm]	57.0 ± 1
s [MN/m]	51.49
δs [MN/m]	5.16
E [M N/m^2]	93.42
δE [M N/m^2]	9.36
R^2	0.87

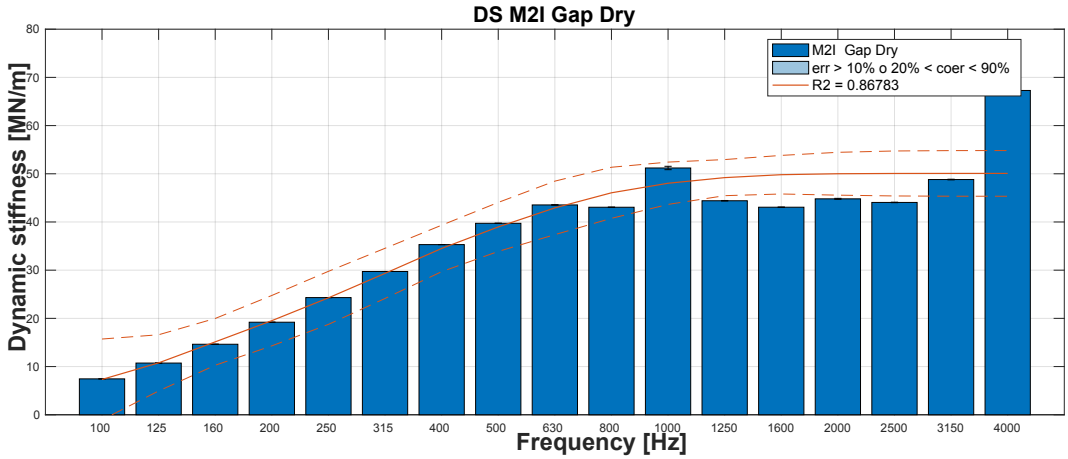

Figure 16. DS third-octave bands spectrum of the M2I sample. Dotted lines represent upper and lower boundary of the confidence interval of the model.

7.3. Results for In Situ Measurements

The in situ measurement was performed in the experimental site of the LIFE E-VIA project located in *"via Paisiello"* in Florence. The pavement tested was an experimental pavement with crumb rubber content.

The DS spectrum has already been presented in Figure 3, while the pavement characteristics and the fit results are reported in Table 10.

Table 10. Technical specifications and DS results of the experimental pavement from the "via Paisiello" site of the LIFE E-VIA project.

	AC6d 5% PFU
Rubber content [%]	5.0
Bitumen content [%]	6.6
Porosity [%]	13.86

Table 10. *Cont.*

	AC6d 5% PFU
Bulk specific gravity	1.980
Maximum gravity	2.299
s [MN/m]	78.96
δs [MN/m]	1.69
R^2	0.99

8. Discussion

From the tests performed to find the critical aspect of the manual non-resonant technique for the DS measurement of pavements emerged that the use of the TAD provides much better results. The interesting parameters of the impact are basically three, the maximum force impressed, and the two angles of incidence with respect to the normal axes of the plane. However, in fields such as the modal analysis and measurement of soft materials according to ISO 9052-1:1989 [31], these parameters do not affect the measure in a way that would invalidate the result.

Investigating the reasons for this difference, it was found that the most critical parameters are the impact angles. Indeed, the linearity test demonstrated that force does not influence the measured SD; therefore, the difficulties in impressing a consistent force by hand is not an issue. The results showed that the non-zero angles of impact occurring in the manual usage of the impact hammer could affect the DS spectrum, resulting in increased uncertainties that are arise while fitting the model. Indeed, with a bigger angle of incidence, the impedance head does not operate properly, as some of the energy is delivered along the orthogonal directions to the head axis. The TAD, by allowing the hammer to be leveled, ensures that it impacts the head surface at a small angle, which remains constant throughout the measurement session. In this way, the TAD maximizes the R^2 and minimizes the confidence interval of the estimated value for the DS of the sample. More importantly, TAD allows us to obtain the DS spectra and the associated uncertainties in accordance with the model proposed in the literature [36].

Regarding the sample fastening method, we tested the possibility of using concrete instead of plaster. In terms of linearity, concrete seems to perform better at 100 N and above, while plaster performs better for lower impressed forces.

Looking at the drying process monitoring results presented in Figure 13, the plaster seems to yield better results in the investigated drying period (from day one to day three). When judging these results, one must considered that the drying performance of plaster and concrete varies considerably based on external temperature and humidity. Indeed, the plaster is advantaged with higher temperatures and lower humidity while the concrete dries faster in high humidity. Thus, the right choice of fastening material depends on the external conditions.

Concerning the hammer tip, Figure 14a shows that negligible differences are present between rubber and nylon tips regardless of the difference indicated by the manufacturer and reported in Table 6. However, the rubber tip was identified as the preferred one due to the lower level of uncertainties associated with the third-octave band's values.

In view of the results from the study on the samples fastening process, it must be underlined that the in-lab measurements are subjected to problems due to the curing time of the cement/plaster and to accidental detachment phenomena that can compromise the measurement. In the case of in situ measurements, the stabilization of the sample is not an issue, so the main criticalities are connected to any slopes in the pavement. When the road has a remarkable donkey saddle profile, non-zero impact angles can occur. In those cases,

the correct alignment of the instrumentation is challenging, and more attention must be paid.

Regarding the impedance head, the presence of the threaded hole on top of the top face generate important variation in the spectrum and higher uncertainties, as shown in Figure 15a. The installation of a metallic interface on top of the head is thus crucial in producing correct DS measurements.

Later, further DS measurements were performed on two other different test pavements, a pavement sample, and a in situ pavement. Those results showed good agreement with the DS model proposed by [36]. Moreover, the absolute DS value and the associated standard deviation are comparable with those obtained by [36] using the shaker. Achieving this low level of uncertainty is a remarkable result for the DS measurement of pavements with impulsive force application. To the knowledge of the authors, this is a novel result, never presented before in the literature.

9. Conclusions

The DS is an essential parameter for the characterization of pavements, not only in terms of durability but also in terms of noisiness. Indeed, different studies suggest a correlation between DS and the noisiness of pavements, suggesting a lower DS is connected to lower levels of TRN. However, the DS measurement is not straightforward because of the typically high level of pavement stiffness. Thus, the measurement technique requires a fine-tuning process. In the literature, the *shaker* is considered to be the reference for those measurements, while the impact hammer is considered incapable of producing acceptable results due to the lower signal-to-noise ratio that is technically achievable. Indeed, using the shaker, some authors obtained good results with a non-resonant technique in measuring the DS of in situ and in-laboratory pavements, proposing a model for the DS spectrum [36].

The present work had the aim of fine-tuning the impact hammer measurement technique for DS to obtain DS spectra analogous to those obtained in the literature with the *shaker*. For this purpose, a low-cost 3D-printed device named TAD was developed to allow for the better control of the force impressed and impact angles, allowing the identification of the parameters have the greatest impact on the quality of the results.

The system, successfully calibrated in the 100–1000 Hz range, was then able to evidence that the most critical aspect of the impact hammer measurements of pavement DS can be found in the manual usage of the hammer, highlighting the strong influence of the impact angles. Consequently, using the TAD, out work focused on optimizing the response detection, also studying the influence of the fastening process (for concrete and plaster), the hammer tip, the applied force, and the presence of asperity on the impact area. This process led to the definition of a final configuration of the system for in situ and in-laboratory measurements. In parallel with the hardware optimization process, the analysis of the results was also improved to bypass the criticality that emerged at high frequencies. In this way, it was possible to successfully perform the fit with the DS model proposed by [36], which as a result, consistent with the literature, was not possible to be obtained by the manual use of the hammer. The developed system was then utilized to perform in situ and in-laboratory DS measurements on rubber-modified bitumen pavement. The results of those measurements confirmed the capability of the system to reproduce the predicted DS spectrum.

In the meantime, some criticalities of the in-laboratory measurements emerged in comparison with the in situ measurements. Indeed, the latter seems to exhibit a wider frequency range and lower oscillations in the spectrum, suggesting the greater reliability of the results. On the other hand, working on finite dimension specimens, in-laboratory

measurements have the advantage of also being able to estimate the Young modulus of the sample.

The optimization work carried out paves the way for the usage of the impact hammer instead of the shaker, with undoubted advantages in terms of investment costs and the required time for perform the measurements. In the future, by using the hammer, it would be possible to carry out larger measurement campaigns to better investigate the dynamic stiffness of pavements.

Either way, while representing an important step forward for pavements' DS measurements with an impact hammer, the present work has some aspects that may benefit from further investigations. For example, the achieved calibration, while consisting of a good starting point and whiel being a good candidate for in situ calibrations, is far from perfect. Indeed, the possibility of extending the calibration interval can be investigated in future studies.

Another aspect that will require future investigations is the direct comparison between the shaker and the TAD results in terms of accuracy and precision.

In future studies, using the developed system, the influence of different parameters on the DS of pavements could be investigated, including the bitumen content, the presence of crumb rubber, the granulometry, and others. For instance, in a forthcoming work, the results of a study on this matter will be presented. Those results will firstly highlight the effect of crumb rubber introduction on DS and secondly highlight the incidence of the crumb rubber introduction process on the level of DS.

Author Contributions: Conceptualization, M.B. and G.L.; methodology, M.B.; software, M.B., E.G. and F.B.; validation, M.B. and E.G.; formal analysis, M.B. and E.G.; investigation, M.B., E.G. and F.B.; resources, F.B. and G.L.; data curation, M.B. and E.G.; writing—original draft preparation, M.B.; writing—review and editing M.B., E.G., F.B. and G.L.; visualization, M.B. and E.G.; supervision, G.L.; project administration, M.B. and F.B.; funding acquisition, G.L. All authors have read and agreed to the published version of the manuscript.

Funding: This research received no external funding.

Institutional Review Board Statement: Not applicable

Informed Consent Statement: Not applicable

Data Availability Statement: The original contributions presented in this study are included in the article. Further inquiries can be directed to the corresponding authors.

Acknowledgments: This work was developed under the project LIFE E-VIA (LIFE18 ENV/IT/000201) and the project LIFE NEREiDE (LIFE15 ENV/IT/000268).

Conflicts of Interest: The authors declare no conflicts of interest.

Abbreviations

The following abbreviations are used in this manuscript:

DS	Dynamic stiffness
MI	Mechanical impedance
TAD	Test automation device
TRN	Tire-road noise

References

1. Babisch, W.; Beule, B.; Schust, M.; Kersten, N.; Ising, H. Traffic noise and risk of myocardial infarction. *Epidemiology* **2005**, *16*, 33–40.
2. Babisch, W.; Swart, W.; Houthuijs, D.; Selander, J.; Bluhm, G.; Pershagen, G.; Dimakopoulou, K.; Haralabidis, A.S.; Katsouyanni, K.; Davou, E.; et al. Exposure modifiers of the relationships of transportation noise with high blood pressure and noise annoyance. *J. Acoust. Soc. Am.* **2012**, *132*, 3788–3808.
3. Vienneau, D.; Schindler, C.; Perez, L.; Probst-Hensch, N.; Röösli, M. The relationship between transportation noise exposure and ischemic heart disease: a meta-analysis. *Environ. Res.* **2015**, *138*, 372–380.
4. Dratva, J.; Phuleria, H.C.; Foraster, M.; Gaspoz, J.M.; Keidel, D.; Künzli, N.; Liu, L.J.S.; Pons, M.; Zemp, E.; Gerbase, M.W.; et al. Transportation noise and blood pressure in a population-based sample of adults. *Environ. Health Perspect.* **2012**, *120*, 50–55.
5. Recio, A.; Linares, C.; Banegas, J.R.; Díaz, J. Road traffic noise effects on cardiovascular, respiratory, and metabolic health: An integrative model of biological mechanisms. *Environ. Res.* **2016**, *146*, 359–370.
6. Van Kempen, E.; Babisch, W. The quantitative relationship between road traffic noise and hypertension: a meta-analysis. *J. Hypertens.* **2012**, *30*, 1075–1086.
7. Jarup, L.; Babisch, W.; Houthuijs, D.; Pershagen, G.; Katsouyanni, K.; Cadum, E.; Dudley, M.L.; Savigny, P.; Seiffert, I.; Swart, W.; et al. Hypertension and exposure to noise near airports: the HYENA study. *Environ. Health Perspect.* **2008**, *116*, 329–333.
8. Basner, M.; Babisch, W.; Davis, A.; Brink, M.; Clark, C.; Janssen, S.; Stansfeld, S. Auditory and non-auditory effects of noise on health. *Lancet* **2014**, *383*, 1325–1332. https://doi.org/10.1016/S0140-6736(13)61613-X.
9. Guski, R.; Schreckenberg, D.; Schuemer, R. WHO Environmental Noise Guidelines for the European Region: A Systematic Review on Environmental Noise and Annoyance. *Int. J. Environ. Res. Public Health* **2017**, *14*, 1539. https://doi.org/10.3390/ijerph14121539.
10. Minichilli, F.; Gorini, F.; Ascari, E.; Bianchi, F.; Coi, A.; Fredianelli, L.; Licitra, G.; Manzoli, F.; Mezzasalma, L.; Cori, L. Annoyance judgment and measurements of environmental noise: A focus on Italian secondary schools. *Int. J. Environ. Res. Public Health* **2018**, *15*, 208.
11. Muzet, A. Environmental noise, sleep and health. *Sleep Med. Rev.* **2007**, *11*, 135–142.
12. The European Parliament and the Council of the European Union. *Directive 2002/49/EC of the European Parliament and of the Council Relating to the Assessment and Management of Environmental Noise*; Technical report; European Union: Brussels, Belgium, 2002.
13. Pavements, T.C.D.R. *Quiet Pavement Technologies*; Technical Report 2013R10EN; World Road Association PIARC: Paris, France, 2013.
14. The Europeean Commission. *EU Green Public Procurement Criteria for Road Design, Construction and Maintenance*; Technical report; The Europeean Commission: Brussels, Belgium, 2016.
15. Sandberg, U.; and Ejmont, J.A. *Tyre/road Noise. Reference Book*; Informex Ejsmont & Sandberg handelsbolag: Kisa, Sweden, 2002; p. 616.
16. Li, T. Influencing Parameters on Tire-Pavement Interaction Noise: Review, Experiments, and Design Considerations. *Designs* **2018**, *2*, 38. https://doi.org/10.3390/designs2040038.
17. Berge, T.; Storeheier, S.A. Low noise pavements in a Nordic climate. Results from a four year project in Norway. In Proceedings of the 38th International Congress and Exposition on Noise Control Engineering 2009, INTER-NOISE 2009, Ottawa, ON, Canada, 23–26 August 2009; Volume 1, pp. 359–367.
18. Li, M.; van Keulen, W.; Ceylan, H.; Cao, D.; van de Ven, M.; Molenaar, A. Pavement stiffness measurements in relation to mechanical impedance. *Constr. Build. Mater.* **2016**, *102*, 455–461. https://doi.org/10.1016/j.conbuildmat.2015.10.191.
19. Bendtsen, H.; Olesen, E.; Pigasse, G.; Andersen, B.; Raaberg, J.; Kalman, B.; Cesbron, J. *Measurements at the Arnakke Test Site with Small PERS Sections*; PERSUADE Report; 2013. Available online: https://scholar.google.com/scholar?hl=zh-CN&as_sdt=0%2C5&q=Measurements+at+the+Arnakke+Test+Site+with+Small+PERS+Sections&btnG= (accessed on 6 November 2024).
20. Bilawchuk, S. Tire noise assessment of Asphalt Rubber Crumb pavement. *Can. Acoust. Acoust. Can.* **2005**, *33*, 37–41.
21. Sandberg, U.; Goubert, L. *PERSUADE—A European Project for Exceptional Noise Reduction by Means of Poroelastic Road Surfaces*; Technical report; Vejdirektoratet: Copenhagen, Denmark, 2011.
22. Sandberg, U.; Goubert, L. Poroelastic road surface (PERS): A review of 30 years of R&D work. In Proceedings of the INTER-NOISE and NOISE-CON Congress and Conference, Osaka, Japan, 4–7 September 2011; Voume 1, pp. 684–691.
23. Storeheier, S. *Preliminary Investigation on a Poroelastic Material Used as a Low Noise Road Surface*; Norwegian Institute of Technology: Trondheim, Norway, 1987.
24. Nilsson, N.A.; Sylwan, O. New vibro-acoustical measurement tools for characterization of poroelastic road surfaces with respect to tire/road noise. In Proceedings of the Tenth International Congress on Sound and Vibration, Stockholm, Sweeden, 7–10 July 2003; pp. 4343–4350.

25. Swieczko-Zurek, B. Biological hazards in low noise, poroelastic road surfaces. In Proceedings of the 20th International Congress on Sound and Vibration 2013, Bangkok, Thailand, 7–11 July 2013; Crocker, M.J., Pawelczyk, M., Paosawatyanyong, B., Eds.; International Institute of Acoustics and Vibrations: Auburn, AL, USA, 2013; Volume 4, pp. 2813–2818. Conference Code: 103420.
26. Van Keulen, W.; Duškov, M. Inventory study of basic knowledge on tyre/road noise. In *Road and Hydraulic Engineering*; Division of Rijkswaterstaat: Delft, The Netherlands; 2005.
27. Van Blokland, G.; Roovers, M. Measurement methods. In *SILVIA Project Report SILVIA-M+ P-015-02-WP2-140705*; European Commission: Brussels, Belgium, 2005.
28. *EN 12697-26:2018*; CEN/TC 227 Road Materials. Standard 00227438. European Committee for Standardization CEN: Brussels, Belgium, 2018.
29. Nguyen, T.H.; Ahn, J.; Lee, J.; Kim, J.H. Dynamic Modulus of Porous Asphalt and the Effect of Moisture Conditioning. *Materials* **2019**, *12*, 1230 https://doi.org/10.3390/ma12081230.
30. Asdrubali, F.; D′Alessandro, F.; Schiavoni, S.; Baldinelli, G. Lightweight screeds made of concrete and recycled polymers: acoustic, thermal, mechanical and chemical characterization. In Proceedings of the 6th Forum Acusticum, Aalborg, Denmark, 27 June–1 July 2011.
31. *ISO 9052-1:1989*; ISO/TC 43/SC 2 Building Acoustics. International Organization for Standardization ISO: Brussels, Belgium, 1989.
32. Vázquez, V.F.; Paje, S.E. Dynamic Stiffness Assessment of Construction Materials by the Resonant and Non-resonant Methods. *J. Nondestruct. Eval.* 2016,*35*, 34. https://doi.org/10.1007/s10921-016-0350-z.
33. Gade, S.; Zaveri, K.; Konstantin-Hansen, H.; Herlufsen, H. *Complex Modulus and Damping Measurements Using Resonant and Non-Resonant Methods*; SAE International: Warrendale, PA, USA, 1995. https://doi.org/10.4271/951333.
34. *ISO 7626-5:2019*; ISO/TC 108 Mechanical Vibration, Shock and Condition Monitoring. International Organization for Standardization ISO: Brussels, Belgium, 2019.
35. *ISO 7626-2:2015*; ISO/TC 108 Mechanical Vibration, Shock and Condition Monitoring. International Organization for Standardization ISO: Brussels, Belgium, 2015.
36. Vázquez, V.F.; Terán, F.; Luong, J.; Paje, S.E. Dynamic stiffness of road pavements: Construction characteristics-based model and influence on tire/road noise. *Sci. Total Environ.* **2020**, *736*, 139597. https://doi.org/10.1016/j.scitotenv.2020.139597.
37. Bonfiglio, P.; Fausti, P. Dynamic stiffness of materials used for reduction in impact noise: Comparison between different measurement techniques. *Acoustica* **2004**, *66*, 1–8.
38. Ooi, L.E.; Ripin, Z.M. Dynamic stiffness and loss factor measurement of engine rubber mount by impact test. *Mater. Des.* **2011**, *32*, 1880–1887. https://doi.org/10.1016/j.matdes.2010.12.015.
39. Vázquez, V.F.; Paje, S.E. Mechanical impedance and CPX noise of SMA pavements. In Proceedings of the Acoustics 2012; d'Acoustique, S.F., Ed.; Nantes, France, April 2012. Available online: https://hal.science/hal-00810767v1 (accessed on 6 November 2024).
40. Bendtsen, H.; Skov, R.S.H.; Andersen, B.; Neidel, A.; Raaberg, J.; Cesbron, J. *Laboratory Measurement on PERS Test Slabs*; Number 513; Vejdirektoratet: Copenhagen, Denmark, 2014. Available online: https://www.vejdirektoratet.dk/udgivelse/laboratory-measurements-pers-test-slabs (accessed on 09 january 2025)
41. Zakaria, N.M.; Yusoff, N.I.M.; Hardwiyono, S.; Mohd Nayan, K.A.; El-Shafie, A. Measurements of the stiffness and thickness of the pavement asphalt layer using the enhanced resonance search method. *Sci. World J.* **2014**, *2014*, 594797. https://doi.org/10.1155/2014/594797.
42. Vázquez, V.F.; Terán, F.; Luong, J.; Paje, S.E. Functional Performance of Stone Mastic Asphalt Pavements in Spain: Acoustic Assessment. *Coatings* **2019**, *9*, 123. https://doi.org/10.3390/coatings9020123.
43. Czech, K.R.; Gardziejczyk, W. Dynamic Stiffness of Bituminous Mixtures for the Wearing Course of the Road Pavement—A Proposed Method of Measurement. *Materials* **2020**, *13*, 1973. https://doi.org/10.3390/ma13081973.
44. Pratico, F.G.; Pellicano, G.; Bolognese, M.; Licitra, G. A Study on Frequency Response Functions in Pavement Engineering. *Balt. J. Road Bridge Eng.* **2023**, *18*, 208–243. https://doi.org/10.7250/bjrbe.2023-18.595.